The International Journal of Advanced Manufacturing Technology (2019) 100:321–332
https://doi.org/10.1007/s00170-018-2749-4

ORIGINAL ARTICLE

Investigation and modeling of microgrooves generated on diamond grinding wheel by abrasive waterjet based on Box–Behnken experimental design

Zhenzhong Zhang[1] · Peng Yao[1] · Chuanzhen Huang[1] · Jun Wang[2] · Donglin Xue[3] · Weijie Deng[3] · Zhiyu Zhang[3]

Received: 10 May 2018 / Accepted: 18 September 2018 / Published online: 24 September 2018

Abstract
Precision profile grinding with textured diamond wheels is an alternative for generating microstructures on the ceramic mold for glass molding. In this work, a novel texturing strategy employing abrasive waterjet for superabrasive grinding wheels was proposed to generate controllable microtexture profile on the diamond wheel surface efficiently. The quadratic backward-eliminated regression models were developed using Box–Behnken response surface design in the abrasive waterjet micromachining of diamond grinding wheel sample. The effect of operating parameters and their interaction on the depth and width of groove were investigated. The surface speed and standoff distance were found to be main controlling variables on the depth and width of groove, respectively. A consistently good agreement was confirmed between the predicted values and the experimental values under acceptable errors.

Keywords Texturing · Box–Behnken design · Abrasive waterjet · Prediction model

Nomenclature

A	Pressure
B	Standoff distance
b_g	Groove width
b_r	Width of the ridge
C	Surface speed
C_0	Replicate number of the central points
d	Diameter of jet
D	Abrasive flow rate
E	Number of passes
h_g	Groove depth
h_r	Height of the ridge
i	Variable
l	Offset distance of the nozzle
m	Number of the factors
N	Number of experiments
x_i	Coded values of independent variable
x_j	The set of model input variables
X_0	Natural value of an independent variable at the center point
X_i	Natural values of independent variable
ΔX_i	Step change of the real value of the variable
Y	Dependent variables
β_0	Intercept
β_i	Coefficient of linear effect
β_{ii}	Coefficient quadratic effect
β_{ij}	Coefficient of interaction effect
ε	Random error
δ	Standoff distance difference

✉ Peng Yao
yaopeng@sdu.edu.cn

[1] Key Laboratory of High Efficiency and Clean Mechanical Manufacture, Ministry of Education, Shandong University, Jinan 250061, Shandong, People's Republic of China

[2] School of Mechanical and Manufacturing Engineering, The University of New South Wales (UNSW), Sydney, NSW 2052, Australia

[3] Key Laboratory of Optical System Advanced Manufacturing Technology, Changchun Institute of Optics, Fine Mechanics and Physics, Chinese Academy of Sciences, Changchun 130033, People's Republic of China

1 Introduction

The need for the micro-lens arrays like the Fresnel lenses, cylindrical lens array, grating array, and pyramid array in optical industry is rapidly growing, because they improve the

properties and the performance of the integrated optical systems [1]. Glass molding has become a key replication-based process to satisfy mass production of these optical elements [2]. Ceramics (e.g., SiC and SiN) are gradually replacing the traditional molds made of steel and aluminum materials due to their superior high-temperature material properties, such as high wear resistance, excellent chemical stability, high thermal conductivity, and high hardness and strength [3]. Meanwhile, due to the high hardness and strength, it is quite difficult to obtain micro-patterns on the surface of ceramic materials. The innovative grinding technology with textured diamond grinding wheels promises a cost-efficient production, which transfers patterns to the ground workpiece to improve its surface functionality [4, 5]. However, it is a challenging task to generate precise wheel profile due to the remarkable resistance property and geometrical limitation, especially for the metal-bonded diamond grinding wheel. Therefore, the texturing process becomes essential for these wheels to ensure the required profile accuracy and efficiency.

To improve the accuracy and efficiency of texturing, several different dressing methods have been utilized aiming to generate structures on grinding wheels including diamond profile roll dressers, single-point (S-P) diamond dressing tools, micro-w-EDM and laser dressing tools. More recently, Denkena presented a straightforward texturing method using a diamond profile roller to grind continuous riblets with a width of 60 μm and a height of 20 μm on the surface of compressor blades [5]. The results showed that the new texturing method using profile rollers with shift kinematic offers a much higher dressing efficiency and greater process stability, compared with those using form rollers. Another kind of textured grinding wheel developed by Mohamed et al. [6] with a single-point diamond dresser can also be employed to create 0.1-mm deep and 0.475-mm wide helically shaped structures around the conventional aluminum oxide grinding wheel surface. These helically shaped circumferential structures can be formed by traversing a rotating grinding wheel across a single-point diamond mounted on the grinding machine table. Oliveira et al. presented a novel dressing technique that inscribes pre-configurable textures on the grinding wheel surface [7]. The technique combines the single-point electromagnetic (EM) shaker with single-point servo method; it allows the monitoring of the contact between the wheel and the dressing tool so that the produced patterns can be visualized in real-time during the texturing process. Chen and Lin [4] proposed a hybrid approach combining microgrinding with micro-w-EDM dressing that is employed to fabricate crisscross microgroove array on optical glass. The width, depth, and surface roughness Ra of the microgrooves are 15 μm, 8 μm, and 0.0577 μm, respectively. The proposed approach currently requires 8 h to produce a wheel tool. Finally, Khangar et al. examined microstructure and microtexture of laser dressed Al_2O_3 wheel [8]. High-power 2.5-kW Nd:YAG laser was used for dressing and subsequently altered grain structure on the surface of the wheel was observed. The laser was applied to irradiate the surface of grinding wheel, to which the laser beam was oriented radially to the surface of the wheel. The wheel is connected to a motor that can index to specific angles. The most significant of this approach is it allows the generation of complex and precise textures. Another laser texturing method utilizing an ultrashort-pulsed picosecond laser is proposed and applied to produce various microstructures on the surface of hybrid bonded CBN grinding tools [9, 10]. The laser process allows to precisely control the dimensions of the generated features. Thereby, different patterns with the equal active tool surface area are produced. However, either a diamond profile roller or single-point (S-P) diamond dressing tools will bring about the rise of texturing cost when applied to the metal-bonded superabrasive wheel. Moreover, potential problems still need to be solved in micro-w-EDM and laser texturing, such as thermal damage of the target surface to be textured, time-consumption, and high-power consumption.

An abrasive waterjet micromachining technology was proposed to implement thermal damage-free and high-efficient dressing of grinding wheel. It has been shown in earlier studies on dressing diamond and Al_2O_3 grinding wheel that this abrasive waterjet technology can dress grinding wheel well and realize thermal damage-free ablation of grinding wheel materials [11, 12]. However, it has been found that this technology is rarely applied in texturing grinding wheel. It is thus essential to extend the process to generate structures on a grinding wheel. A preliminary result shows that the wheel topography with high protrusion height of grains can be obtained when using the abrasive waterjet machining technology to dress metal-bonded diamond grinding wheel [13]. To achieve controlled profile of textured wheel, it is necessary to understand how the input parameters influence the material removal process. Moreover, the texture of the grinding wheel primarily dominates the production of the patterned workpiece surface. In order to quantify the process of feature transfer from the grinding wheel to the workpiece, it is essential to model the mathematical profile of the dressed grinding wheel.

In abrasive waterjet micromachining, numerous numbers of factors and interactions are there to be considered during machining [14–16]. Conventional designing methods are time-consuming and massive, especially for large quantity of variables. Response surface methodology (RSM) is a collection of statistical and mathematical methods for designing experiments. Box–Behnken design (BBD) approach, one of the response surface methodology, was widely applied in various experiments [17, 18], which has the following advantages: BBD design is not only effective in predicting the response of the fitted model with the least amount of experiments but also contributes to further analysis of the interactions between different variables. Furthermore, it can estimate

the factors of quadratic model efficiently and avoid treatment combinations at an extreme range. In this technique, the main purpose is to investigate and quantify the relationship between the operating parameters and the groove geometry, especially for the interactive effect of multi-parameters on the results.

A novel approach was proposed to generate microstructures on a metal-bonded diamond grinding wheel by on-machine abrasive waterjet micromachining in this research. The objective of this research is to predict the key profile parameters, including groove depth and groove width, of the grooves on the metal-bonded grinding wheels textured by abrasive waterjet. The significance of the abrasive waterjet processing parameters on the machining results will be analyzed through the analysis of variance (ANOVA). At the same time, BBD response surface methodology was applied to investigate the effect and the interaction of the operating process parameters. Moreover, the quadratic backward-eliminated regression models were developed. Finally, the validity of the developed models was verified.

2 Experimental materials and methods

2.1 Experimental set up

On-machine abrasive waterjet micromachining was used to generate microstructures in a metal-bonded diamond grinding wheel. As illustrated schematically in Fig. 1, the high-velocity abrasive waterjet was focused and ejected to the target diamond grinding wheel from the abrasive waterjet nozzle in a radial mode at a standoff distance. An abrasive waterjet micromachining system was used to generate the Gaussian bell-shaped groove on the working surface of the grinding wheel. The groove depth of h_g and groove width of b_g were taken as the characteristic dimension of the profile of processed grooves, which were used to model the groove shape as the main parameters by Alberdi [19]. Developing an analytical model of groove geometry would help to describe an actual profile at work in the texturing process. Figure 1 shows the geometry details of the residual grooves and ridges generated by abrasive waterjet micromachining, which has a groove depth of h_g and a groove width of b_g. The height of the ridge on the grinding wheel is expressed as follow:

$$h_r = h_g \tag{1}$$

The width of the ridge is calculated by:

$$b_r = l - b_g \tag{2}$$

where l represents offset distance of the abrasive waterjet nozzle.

Experiments were initially carried out using a diamond wheel sample in order to develop the model of the groove depth and width precisely and efficiently. As illustrated in Fig. 1. The standoff distance difference δ between p and q is calculated by:

$$\delta = r - r\cos\theta \approx 0.001 \text{ mm} \tag{3}$$

where r is the radius of the grinding wheel; θ is the semi-included angle of jet contact arc, which can be given by $\theta =$

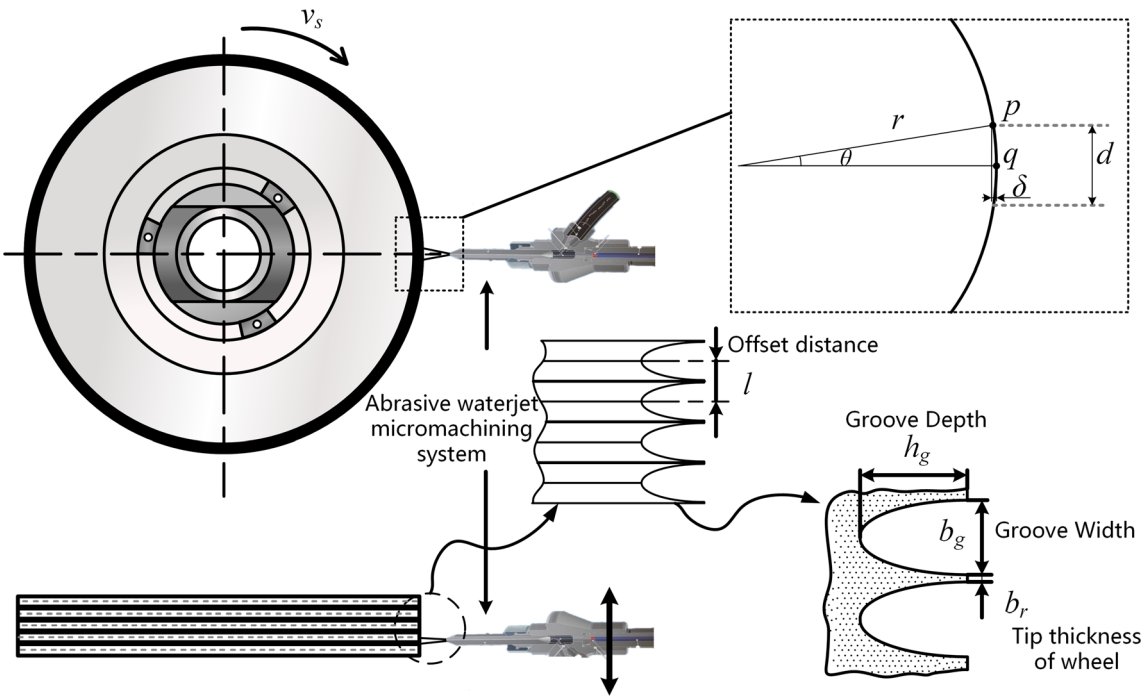

Fig. 1 Illustration of the texturing procedure and groove geometry

$\sin^{-1}(d/2r)$, where d is the diameter of jet; in this paper, it is about 1 mm. The value of δ is far less than 1 mm (the minimum value standoff distance chosen in the experiment). Hence, the change of standoff distance along the grooves can be ignored by linear movement of the table. Based on this rationale, an abrasive waterjet micromachining system was established, as shown in Fig. 2. It mainly consisted of three units, i.e., an ultra-precision motion and servo control platform, a pressurized water supplier, and an abrasive waterjet nozzle. The sample was clamped on an ultra-precision surface grinding machine NAS520 CNC. The kinematics for generating the texturing involve a relative movement between the abrasive waterjet nozzle and the sample. The texturing process was performed by feeding the machine table in reciprocating movement. Straight grooves were the texturing conditions are listed in Table 1. Five principal machining parameters,

Table 1 Abrasive waterjet texturing parameters

Texturing condition	
Wheel sample characteristics	
Grain	Diamond
Grit size	1500# (10 μm)
Bond	Bronze
Abrasive waterjet characteristics	
Abrasive material	Garnet
Abrasive particle size	150# (75 to106 μm)
Orifice diameter	0.25 mm
Nozzle diameter	0.76 mm

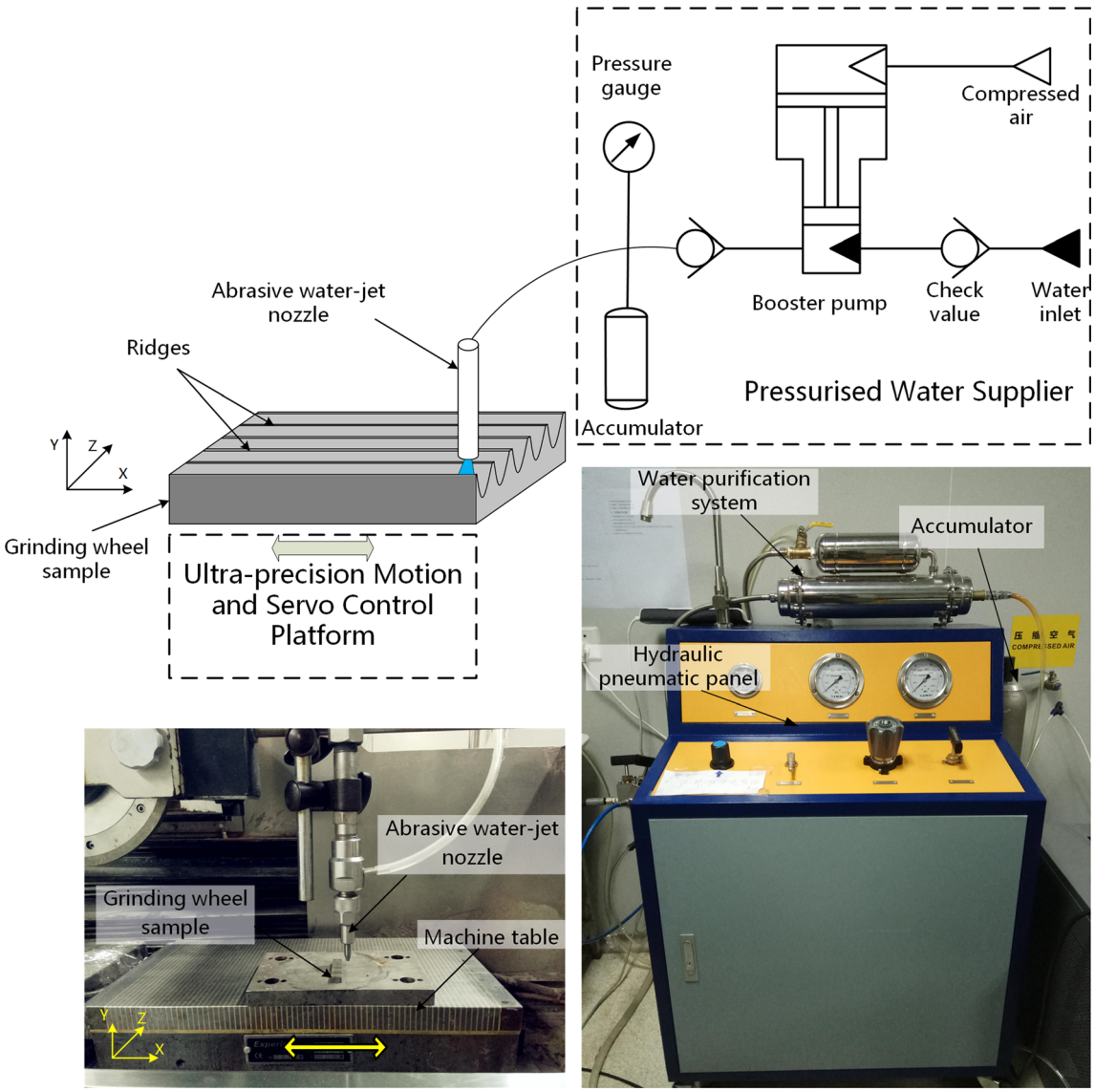

Fig. 2 Schematic of the grinding wheel sample during abrasive waterjet texturing and experimental setup

including pressure (Mpa), standoff distance (mm), surface speed (mm/s), abrasive flow rate (g/min), and number of passes are employed to investigate the influence of machining parameters on the groove geometry.

The depth and width of groove were measured with the three-dimensional (3D) laser scanning confocal microscope (Keyence VK-X200K). Scanned (3D) image of groove is shown in Fig. 3a and scanned section profile of the machined surface is shown in Fig. 3b.

2.2 Design of experiments

The design procedure of RSM for microgroove modeling is as follows [20]:

(i) Identifying the important controlling variables of abrasive waterjet and finding the upper and lower limits of them.
(ii) Designing and conducting the texturing experiments.
(iii) Developing a mathematical model of the groove geometry with the best fittings.
(iv) Representing the direct and interactive effects of process parameters through two and three-dimensional plots.
(v) Analysis of results.

In the current study, by employing the Box–Behnken experiment design, the effect of the five independent variables on the responses was investigated. Experiments were established based on a BBD with five factors at three levels as listed in Table 2, and each independent variable was studied at three levels, coded as − 1, 0, and + 1 for low, middle, and high concentrations, respectively. The coding of the variables was done by the following equation:

$$x_i = \frac{X_i - X_0}{\Delta X_i} \quad i = 1, 2, 3, \cdots m \tag{4}$$

where x_i and X_i are the coded and natural values of independent variable, respectively, X_0 is the natural value of an independent variable at the center point, and ΔX_i is the step change of the real value of the variable i corresponding to a variation of a unit for the dimensionless value of the variable i.

Total 46 experiments were embodied in the design. In order to allow the estimation of pure error, the designed experiments were performed with six center points. It enables the response function at intermediate levels to be calculated and allows the system performance at any experimental point to be evaluated within the scope of the study. The number of experiments (N) is usually defined as follows:

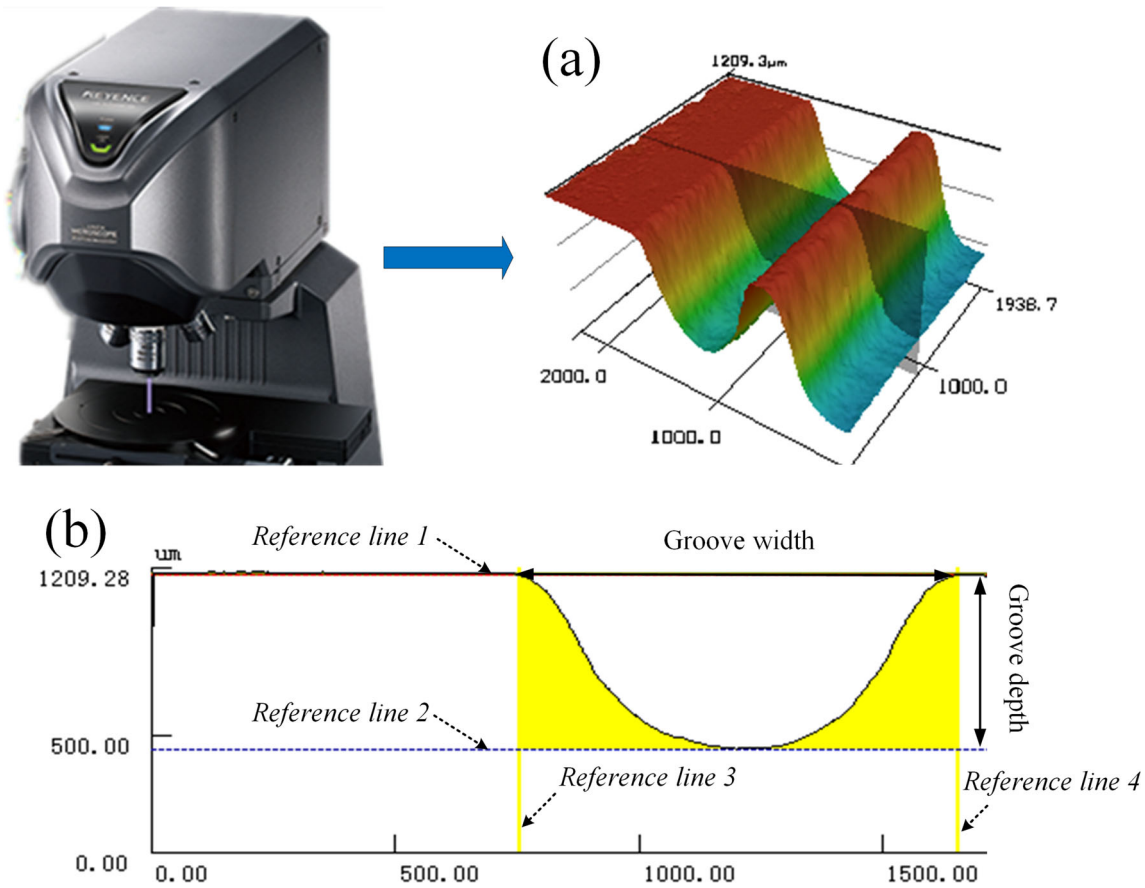

Fig. 3 3D laser scanning confocal microscope. **a** 3D scanned image of groove. **b** Scanned section profile of the machined surface

Table 2 Experimental ranges and levels of the respective independent variables

Independent variables	Factor level		
	−1	0	1
A, the pressure (MPa)	30	40	50
B, the standoff distance (mm)	1	3	5
C, the surface speed (mm/s)	170	280	390
D, the abrasive flow rate (g/min)	8	16	24
E, the number of passes	200	400	600

$$N = 2m(m-1) + C_0 \tag{5}$$

where m is number of the factors and C_0 is the replicate number of the central points.

Following second order polynomial, (Eq. (6)) was used to fit the results and correlate the relationship between the operating parameters and the groove geometry. Considering all the linear terms, square terms, and interaction items, the quadratic response model can be described as:

$$Y = \beta_0 + \sum_{i=1}^{m} \beta_i x_i + \sum_{i=1}^{m} \beta_{ii} x_i^2 + \sum_{i<j}^{m} \beta_{ij} x_i x_j + \varepsilon \tag{6}$$

where Y represents the responses (dependent variables); x_i and x_j are the set of model input variables (i and j range from 1 to m); β_0 is the intercept; β_i and β_{ii} are coefficients of linear and quadratic effect, respectively; β_{ij} is the coefficient of interaction effect; m is the number of input variables ($m = 5$ in this study); and ε is the random error.

The analyses of RSM and developing of models were carried out using the Design Expert software (Stat-Ease Inc., Minneapolis, MN, USA).

3 Results and discussion

3.1 Model building and statistical significance test

Typical groove topography and section profiles in diamond grinding wheel sample are shown in Fig. 4. The grooves created can be approximated as in the Gaussian bell shape. It can be observed that the higher groove depth can be obtained at a smaller standoff distance and a higher number of passes (Fig. 4a–c). Compared to the groove depth, the groove width changes insignificant. The reason is described in detail later. All results obtained from BBD experimental design are summarized in Table 3. From these data, the quadratic backward-eliminated regression models of groove depth (h_g, μm) and width (b_g, μm) are developed as:

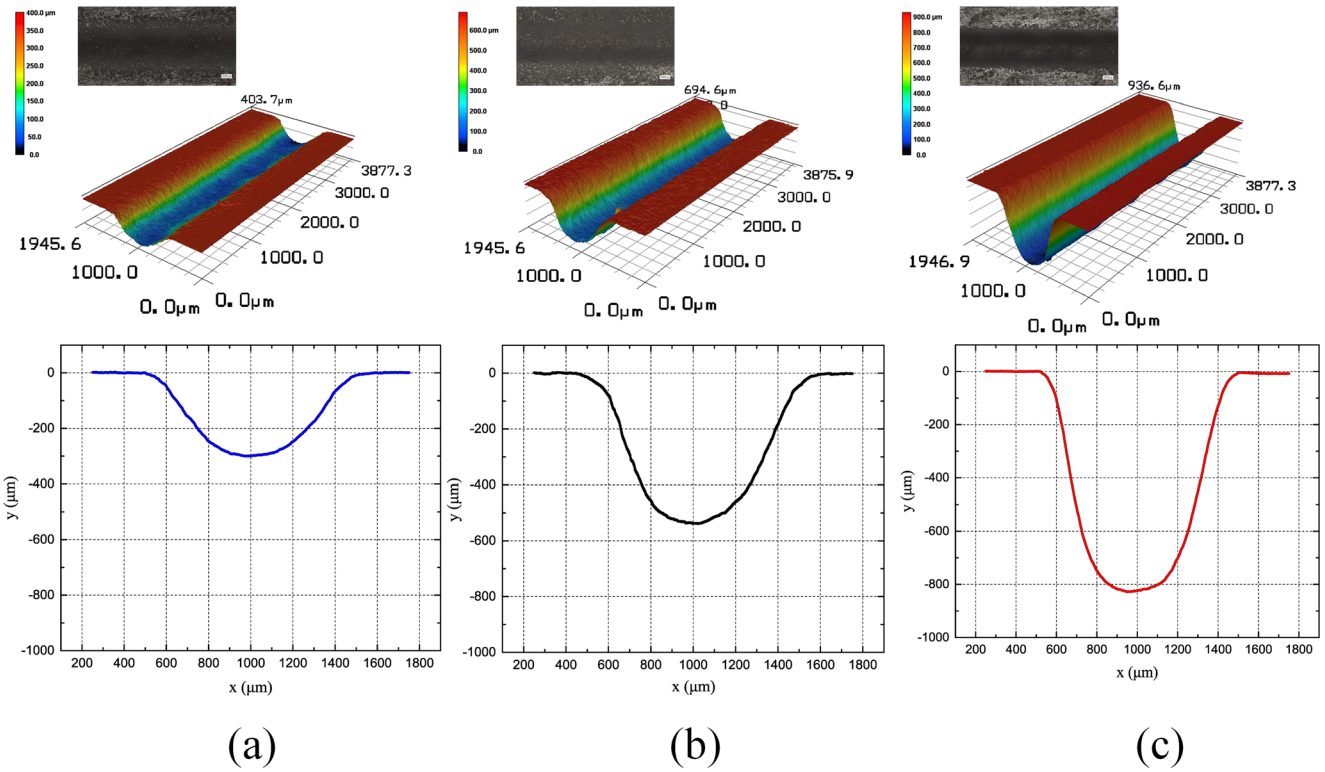

Fig. 4 Typical groove topography and section profiles in diamond grinding wheel sample at different standoff distances (B), abrasive flow rate (D), and the number of passes (E) (pressure $A = 40$ MPa surface speed C = 280 mm/s). **a** $B = 5$ mm, $D = 16$ g/min, $E = 200$, **b** $B = 5$ mm, $D = 8$ g/min, $E = 400$, **c** $B = 3$ mm, $D = 16$ g/min, $E = 400$

Table 3 BBD design and experimental results

Std	Run	Factor 1 *A*, pressure, (MPa)	Factor 2 *B*, standoff distance (mm)	Factor 3 *C*, surface speed (mm/s)	Factor 4 *D*, abrasive flow rate (g/min)	Factor 5 *E*, number of passes	Response 1 Depth (μm)	Response 2 Width (μm)
29	1	40.00	3.00	170.00	16.00	200.00	809.73	993.76
8	2	40.00	3.00	390.00	24.00	400.00	600.17	988.57
14	3	50.00	3.00	170.00	16.00	400.00	1470.52	1021.77
35	4	30.00	3.00	280.00	16.00	600.00	894.98	1088.58
39	5	40.00	1.00	280.00	24.00	400.00	1176.05	846.32
4	6	50.00	5.00	280.00	16.00	400.00	864.22	1117.83
26	7	50.00	3.00	280.00	8.00	400.00	541.8	957.05
41	8	40.00	3.00	280.00	16.00	400.00	825.33	980.17
33	9	30.00	3.00	280.00	16.00	200.00	371.46	898.73
9	10	40.00	1.00	280.00	16.00	200.00	449.81	822.25
36	11	50.00	3.00	280.00	16.00	600.00	1223.18	1000.85
43	12	40.00	3.00	280.00	16.00	400.00	748.45	943.27
22	13	40.00	5.00	170.00	16.00	400.00	1274.7	1121.44
45	14	40.00	3.00	280.00	16.00	400.00	718.4	966.85
7	15	40.00	3.00	170.00	24.00	400.00	2030.33	992.8
42	16	40.00	3.00	280.00	16.00	400.00	900.97	979.95
30	17	40.00	3.00	390.00	16.00	200.00	485.92	936.75
32	18	40.00	3.00	390.00	16.00	600.00	899.95	987.09
25	19	30.00	3.00	280.00	8.00	400.00	405.03	954.43
23	20	40.00	1.00	390.00	16.00	400.00	406.1	817.5
19	21	40.00	3.00	280.00	8.00	600.00	336.38	912.38
18	22	40.00	3.00	280.00	24.00	200.00	438.95	898.26
12	23	40.00	5.00	280.00	16.00	600.00	787.74	1110.17
40	24	40.00	5.00	280.00	24.00	400.00	711.94	1110.96
10	25	40.00	5.00	280.00	16.00	200.00	290.6	1003.53
3	26	30.00	5.00	280.00	16.00	400.00	402.26	1094.08
34	27	50.00	3.00	280.00	16.00	200.00	418.21	933.91
11	28	40.00	1.00	280.00	16.00	600.00	1100.99	891.91
27	29	30.00	3.00	280.00	24.00	400.00	871.25	960
1	30	30.00	1.00	280.00	16.00	400.00	894.76	841.08
38	31	40.00	5.00	280.00	8.00	400.00	529.05	1095.24
15	32	30.00	3.00	390.00	16.00	400.00	603.28	934.6
44	33	40.00	3.00	280.00	16.00	400.00	745.4	995.28
6	34	40.00	3.00	390.00	8.00	400.00	483.2	937.36
37	35	40.00	1.00	280.00	8.00	400.00	603.53	822.74
17	36	40.00	3.00	280.00	8.00	200.00	367.16	943.27
16	37	50.00	3.00	390.00	16.00	400.00	901.07	982.15
28	38	50.00	3.00	280.00	24.00	400.00	1240.94	970.08
2	39	50.00	1.00	280.00	16.00	400.00	991.41	844.3
20	40	40.00	3.00	280.00	24.00	600.00	1715.3	1016.63
21	41	40.00	1.00	170.00	16.00	400.00	1747.48	839.06
13	42	30.00	3.00	170.00	16.00	400.00	1440.09	982.57
31	43	40.00	3.00	170.00	16.00	600.00	2409.95	1011.05
5	44	40.00	3.00	170.00	8.00	400.00	1253.21	998.96
46	45	40.00	3.00	280.00	16.00	400.00	942.58	991.14
24	46	40.00	5.00	390.00	16.00	400.00	924.79	1150.26

Table 4 ANOVA for quadratic backward-eliminated regression models

Source	Sum of squares	DOF	Mean square	F value	p value, Prob > F	
For depth						
Model	9,199,853.47	10	919,985.35	53.73	< 0.0001	Significant
Residual	599,254.77	35	17,121.56			
Lack of fit	556,889.06	30	18,562.97	2.19	0.1947	Not significant
Pure error	42,365.72	5	8473.14			
Adj $R^2 = 0.9214$						
Pred $R^2 = 0.8728$						
Adeq precision = 30.1371						
For width						
Model	3.024E+ 005	6	50,395.65	65.09	< 0.0001	Significant
Residual	30,193.69	39	774.20			
Lack of fit	28,404.86	34	835.44	2.34	0.1743	Not significant
Pure error	1788.83	5	357.77			
Adj $R^2 = 0.8952$						
Pred $R^2 = 0.8594$						
Adeq precision = 30.709						

$$h_g = 750.27 + 110.51A - 99.05B - 445.72C + 266.60D + 358.54E + 247.87BC - 165.04CD - 296.55CE + 326.78DE + 358.51C^2 \quad (7)$$

$$b_g = 971.46 + 4.62A + 129.90B - 14.20C + 10.14D + 36.76E + 37.31DE \quad (8)$$

where, A, B, C, D, and E represent the pressure (Mpa), standoff distance (mm), surface speed (mm/s), abrasive flow rate(g/min), and number of passes, respectively.

The insignificant model terms are reduced to improve the models. Analysis of variance (ANOVA) is required then to evaluate the significance of the regression coefficients by their corresponding F values which are listed in Table 4. This selected model is significant due to the model F value, 53.73 for depth and 65.09 for width. There is only a 0.01% chance than a "model F value" this large might occur because of noise, which manifested that there was no obvious fitting error in the model. The lack of fit, 2.19 for depth and 2.34 for width, is relative to a pure error. This clearly states that the model perfectly fits into the experimental data. The fitness of the model was further confirmed by estimating the adjusted R^2 and the predicted R^2. The Pred R^2 values (0.8728 for depth, 0.8594 for width) are in reasonable agreement with the Adj R^2 (0.9214 for depth, 0.8952 for width), because the difference between them was within 0.2. Adequate precision estimates the signal to noise ratio and an A ratio exceeding 4 is desirable. The measurement of the signal to noise ratio resulted in 30.1371 and 30.709, respectively, implying an adequate precision ratio. Hence, this model could be employed to navigate the response surface design space.

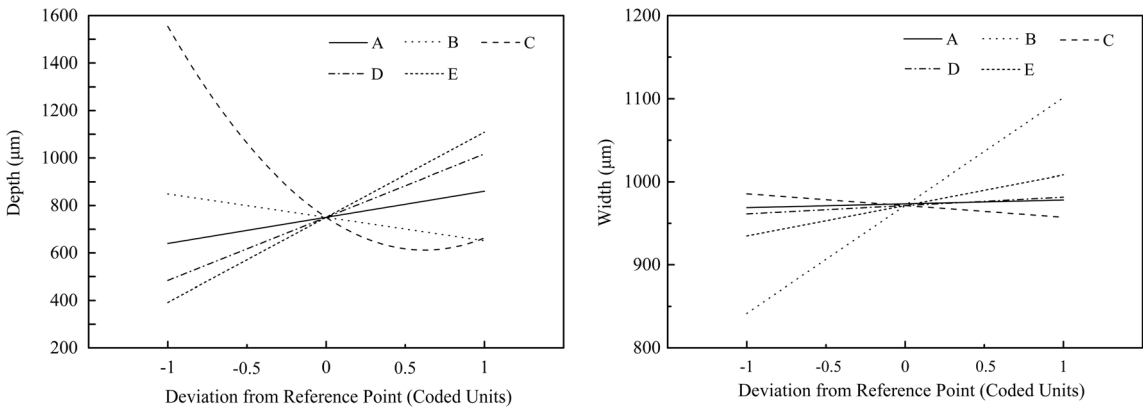

Fig. 5 Perturbation plot showing the effect of all factors on **a** groove depth and **b** groove width (A pressure (MPa), B standoff distance (mm), C surface speed (mm/s), D abrasive flow rate (g/min), E number of passes)

3.2 Effects of each factor

Perturbation plots, as shown in Fig. 5, illustrated the effects of operating parameters on groove depth and width. The response to single factor was plotted by only changing the factor within its range while the other factors are set to constant at the reference value. As shown in Fig. 5a, the most influential factor on depth was found as the surface speed (factor C) for the proposed model; the depth decreases with an increase in surface speed, but the rate of decrease in the depth declines. This finding may be attributed to the fact that the increased surface speed limited the number of particles impinging on target area per unit time. The relations between depth and the other factors such as *A*, *D*, and *E* follow some trends with different gradients, which linearly increase as these factors increase. It was also noticed that the standoff distance (factor *B*) has an opposite effect on depth. This may be due to the lower impinging energy caused by the increase of standoff distance.

As shown in Fig. 5b, it is clear that the standoff distance (factor *B*) is the most influential factor on width followed by *E* and *D*. When the standoff distance increases from 1 to 3 mm, the width increases. The results are in agreement with Karakurt [21] who clearly indicated that an increase in the standoff distance leads to the divergence of the jet, which causes larger cutting widths. Moreover, there is no substantial change in degree of the width in range of the waterjet pressure (factor *A*). These were consistent with the literature [22], since they found no remarkable relationship between water pressure and cutting width. As can be seen, an increase in the surface speed (factor *C*) from 170 to 390 mm/s leads to the decrease of the width, which may be related to the impinging jet energy

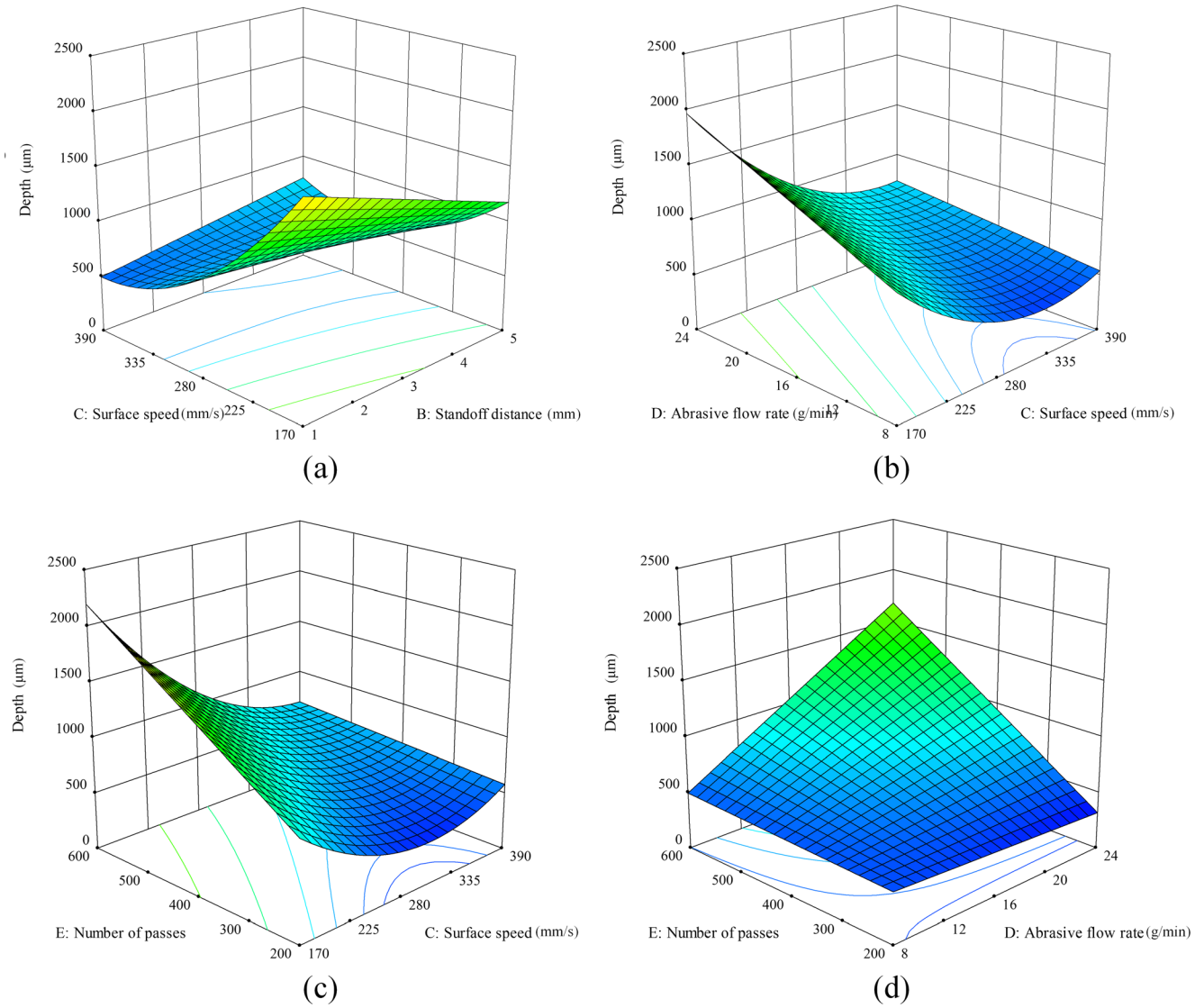

Fig. 6 3D surface plots of groove depth as a function of **a** standoff distance and surface speed, **b** surface speed and abrasive flow rate, **c** surface speed and number of passes, and **d** abrasive flow rate and number of passes

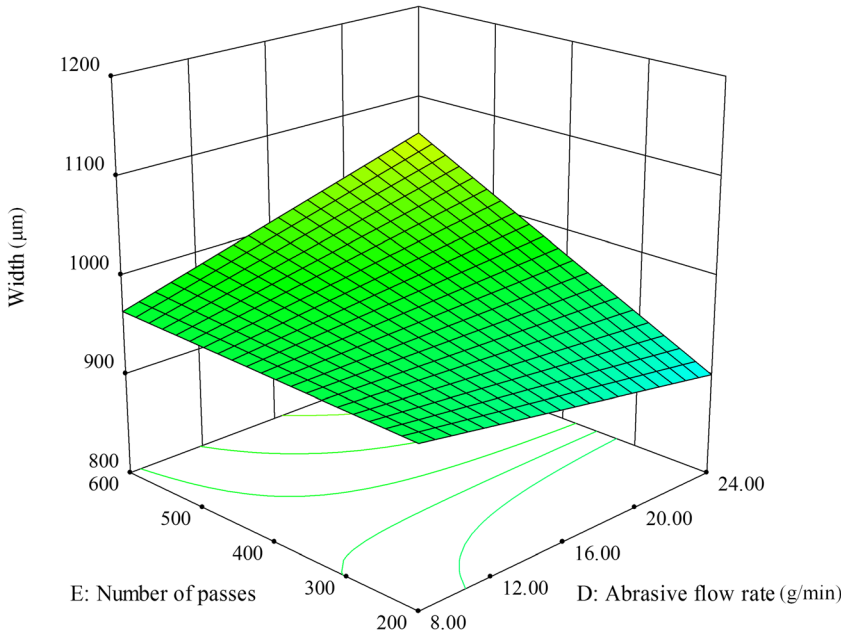

Fig. 7 3D surface plots of groove width as a function of abrasive flow rate and number of passes

levels. The jet loses its energy rapidly with a reduction in the jet exposure time on the workpiece, which leads to a decrease in the width as is in the present study.

3.3 Effects of interaction between factors

The effects of each two independent variables (by keeping the other at central level) and their interactions in responses (The depth and width) can be best interpreted by the three-dimensional (3D) response surface and contour plots as shown in Figs. 6 and 7, respectively. According to Fig. 6a–c, the deeper groove can be acquired at a lower surface speed combined with a smaller standoff distance or a higher abrasive flow rate or a higher number of passes, which is in consistence with the results in turning of alumina ceramics using abrasive waterjet. [18] The effects of surface speed on the depth can be justified based on the facts mentioned in Section 3.2. Figure 6d demonstrates the binary interaction of the number of passes and abrasive flowrate. The depth increased severely by raising the number of passes. Furthermore, the depth increased with the increase of abrasive flow rate, due to the supply of more destruction energy. From Fig. 7, it can be observed that the wider groove can be obtained at a higher number of passes and a higher abrasive flow rate. One reason may be the linear relationship between the number of passes and exposure time. Previously, Srinivasu et al. [23] also reported the influence of multi-pass on kerf generation. They found that a longer time of the jet exposing onto the material leads to more particles contributing to material removal in a given target area. The observed trend also might be owing to the abrasive flow rate on the erosion energy. When the abrasive flow rate was 8 g/min, the trend of groove width varied with the number of passes was not significant. It is implicit that a critical energy to fracture the material, below which any increase in passes, does not have an effect on the groove width. This observation conformed to the previous finding as reported in the literatures [24].

3.4 Validation of the developed models

The developed models are verified by experiments at various cutting conditions given in Table 5, in which the parameter

Table 5 Verification experiments

Run	Pressure (MPa)	Standoff distance (mm)	Surface speed (mm/s)	Abrasive flow rate (g/min)	Number of passes
1	40.00	2.00	225.00	14.50	360.00
2	35.00	4.20	280.00	17.00	420.00
3	42.00	3.60	170.00	16.50	240.00
4	32.00	1.50	280.00	9.50	500.00
5	45.00	3.00	170.00	22.00	200.00
6	40.00	1.80	280.00	20.00	480.00

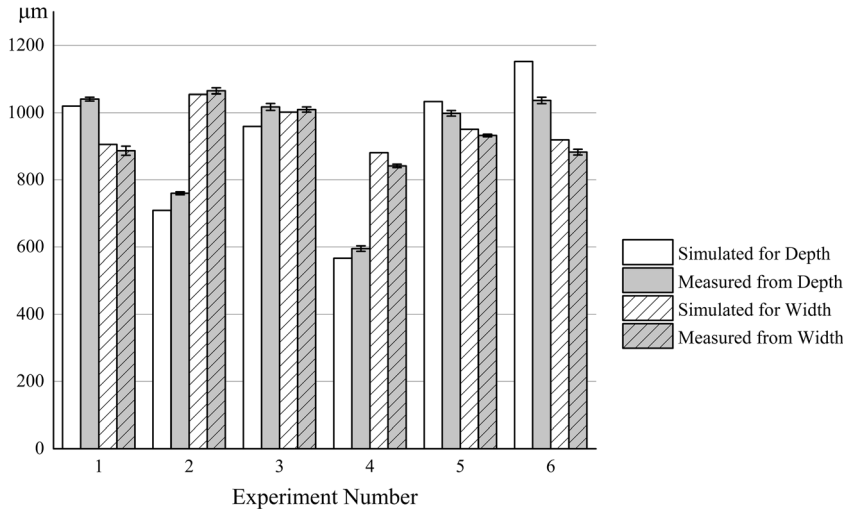

Fig. 8 Comparison of groove depth and width derived from verification experiments and model predictions

combinations were set randomly in the range of the models. The comparison between experimental results and model prediction results derived from the Eq. (7) and Eq. (8) is shown in Fig. 8. The average percentage of error in the groove depth was 5.6%, while the average percentage of error in the groove width was 2.4%. Good agreement between predicted and measured was obtained. As a result, the models from BBD are considered to be accurate and reliable for predicting the depth and width.

4 Conclusions

The main scope of this paper was to propose and validate a quadratic backward-eliminated regression model that is suitable for devising the superabrasive grinding wheel texturing strategies. The application of abrasive waterjet has been previously tested on the machining of other materials, but never been applied in a single study for the wheel texturing in the open literature. The research aims to provide new dressing technology to generate microgrooves on diamond grinding wheel by abrasive waterjet.

The following conclusions can be drawn:

(1) The Box–Behnken experimental design was used to understand the effect of the process parameters on the groove depth and width. To control the geometry of groove, the pressure, standoff distance, surface speed, abrasive flow rate, and number of passes were studied as process parameters. The model equations representing the depth and width of groove were expressed as functions of five operating parameters.

(2) The analysis of variance (ANOVA) showed a good fit of the experimental data to the quadratic backward-eliminated regression models. The developed models are significant with high-adjusted correlation coefficients: 0.9214 for depth and 0.8952 for width.

(3) The perturbation plot revealed that the surface speed is the most significant factor influencing the groove depth. Moreover, the groove width was highly influenced by the standoff distance. On the other hand, the curvature shapes of response surface and contour plots clearly represent effects of their interactions on responses.

(4) The models were verified with experimental results of grooves generated at different conditions. The verification results showed that the average prediction errors of the models for groove depth and groove width were 5.6% and 2.4%, respectively. These results showed that predicted values were found to be accorded with experimental values very well, revealing the suitability of the chosen model. Therefore, the reliability of this model using Box–Behnken design was proven to be reasonably accurate for prediction in the limited range as investigated in this study.

Although further challenges in modeling of microgrooves exist (e.g., limited range, wheel sample dressing process), the proposed model is regarded as an enabling step for the generation of controllable microgroove profile on the diamond wheel surface efficiently by choosing proper abrasive waterjet process parameters.

Funding information This work was supported by National Natural Science Foundation of China (No. 51875321), Shandong Province Natural Science Foundation (Grant No. ZR2018MEE019, ZR2018ZB0521) and Key Laboratory of Optical System Advanced Manufacturing Technology (Grant No. Y6SY1FJ160).

References

1. Brinksmeier E, Riemer O, Gläbe RM: Fabrication of complex optical components. Springer Berlin Heidelberg, 2013
2. Zhou TF, Liu X, Liang Z, Liu Y, Xie J, Wang X (2017) Recent advancements in optical microstructure fabrication through glass molding process. Front Mech Eng 12:46–65
3. Guo B, Zhao QL (2017) Ultrasonic vibration assisted grinding of hard and brittle linear micro-structured surfaces. Precis Eng 48:98–106
4. Chen S, Lin S (2011) Development of an extremely thin grinding-tool for grinding microgrooves in optical glass. J Mater Process Technol 211:1581–1589
5. Denkena B, Köhler J, Wang B (2010) Manufacturing of functional riblet structures by profile grinding. CIRP J Manuf Sci Technol 3:14–26
6. Mohamed AO, Bauer R, Warkentin A (2013) Application of shallow circumferential grooved wheels to creep-feed grinding. J Mater Process Technol 213:700–706
7. Oliveira JFG, Bottene AC, França TV (2010) A novel dressing technique for texturing of ground surfaces. CIRP Ann Manuf Technol 59:361–364
8. Khangar A, Dahotre NB (2005) Morphological modification in laser-dressed alumina grinding wheel material for microscale grinding. J Mater Process Technol 170:1–10
9. Walter C, Komischke T, Kuster F, Wegener K (2014) Laser-structured grinding tools – generation of prototype patterns and performance evaluation. J Mater Process Technol 214:951–961
10. Walter C, Komischke T, Weing Rtner E, Wegener K (2014) Structuring of CBN grinding tools by ultrashort pulse laser ablation. Procedia CIRP 14:31–36
11. Yao P, Wang W, Huang CZ, Wang J, Zhu HT, Zhang ZY (2014) High efficiency abrasive waterjet dressing of diamond grinding wheel. Adv Mater Res 1017:243–248
12. Shen JY, Xu XP, Lin B, Xu YS (2001) Lap-grinding of Al_2O_3 ceramics assisted by water-jet dressing metal bond diamond wheel. Key Eng Mater 202-203:171–176
13. Zhang ZZ, Yao P, Zhang ZY, Xue DL, Wang C, Huang CZ, Zhu HT (2017) A novel technique for dressing metal-bonded diamond grinding wheel with abrasive waterjet and touch truing. Int J Adv Manuf Technol 93:3063–3073
14. Qi H, Wen D, Yuan Q, Zhang L, Chen Z (2017) Numerical investigation on particle impact erosion in ultrasonic-assisted abrasive slurry jet micro-machining of glasses. Powder Technol 314:627–634
15. Cai DH, Qi H, Wen DH, Zhang L, Yuan QL, Chen ZZ (2016) Effect of fluid motion on the impact erosion by a micro-particle on quartz crystals. AIP Adv 6:85203–085203-11
16. Yang M, Li C, Zhang Y, Jia D, Zhang X, Hou Y, Li R, Wang J (2017) Maximum undeformed equivalent chip thickness for ductile-brittle transition of zirconia ceramics under different lubrication conditions. Int J Mach Tools Manuf 122:55–65
17. Ferreira SLC, Bruns RE, Ferreira HS, Matos GD, David JM, Brandão GC, Da Silva EGP, Portugal LA, Dos Reis PS, Souza AS, Dos Santos WNL (2007) Box-Behnken design: an alternative for the optimization of analytical methods. Anal Chim Acta 597:179–186
18. Liu D, Huang CZ, Wang J, Zhu HT, Yao P, Liu ZW (2014) Modeling and optimization of operating parameters for abrasive waterjet turning alumina ceramics using response surface methodology combined with Box–Behnken design. Ceram Int 40:7899–7908
19. Alberdi A, Rivero A, de Lacalle LNL, Etxeberria I, Suárez A (2010) Effect of process parameter on the kerf geometry in abrasive water jet milling. Int J Adv Manuf Technol 51:467–480
20. Gunaraj V, Murugan N (1999) Application of response surface methodology for predicting weld bead quality in submerged arc welding of pipes. J Mater Process Technol 88:266–275
21. Karakurt I, Aydin G, Aydiner K (2014) An investigation on the kerf width in abrasive waterjet cutting of granitic rocks. Arab J Geosci 7: 2923–2932
22. Chung Y, Geskin ES, Singh PJ (1992) Prediction of the geometry of the kerf created in the course of abrasive waterjet machining of ductile materials. In: Springer Netherlands
23. Shanmugam DK, Masood SH (2009) An investigation on kerf characteristics in abrasive waterjet cutting of layered composites. J Mater Process Technol 209:3887–3893
24. Dadkhahipour K, Nguyen T, Wang J (2012) Mechanisms of channel formation on glasses by abrasive waterjet milling. Wear 292–293:1–10